ChemPubSoc Europe

DOI: 10.1002/open.201900119

Open Access ChemistryOPEN Full Papers

gem-Diethyl Pyrroline Nitroxide Spin Labels: Synthesis, EPR Characterization, Rotamer Libraries and Biocompatibility

Stephanie Bleicken,[a, c] Tufa E. Assafa+,[a] Hui Zhang+,[b] Christina Elsner,[a] Irina Ritsch,[d] Maren Pink,[e] Suchada Rajca,[b] Gunnar Jeschke,[d] Andrzej Rajca,*[b] and Enrica Bordignon*[a]

The availability of bioresistant spin labels is crucial for the optimization of site-directed spin labeling protocols for EPR structural studies of biomolecules in a cellular context. As labeling can affect proteins' fold and/or function, having the possibility to choose between different spin labels will increase the probability to produce spin-labeled functional proteins. Here, we report the synthesis and characterization of iodoacetamide- and maleimide-functionalized spin labels based on the *gem*-diethyl pyrroline structure. The two nitroxide labels are compared to conventional *gem*-dimethyl analogs by site-directed spin labeling (SDSL) electron paramagnetic resonance (EPR) spectroscopy, using two water soluble proteins: T4 lysozyme and Bid. To foster their use for structural studies, we also present rotamer libraries for these labels, compatible with the MMM software. Finally, we investigate the "true" biocompatibility of the *gem*-diethyl probes comparing the resistance towards chemical reduction of the NO group in ascorbate solutions and *E. coli* cytosol at different spin concentrations.

Introduction

Site-directed spin labeling (SDSL) electron paramagnetic resonance (EPR) spectroscopy is a biophysical technique based on the site-specific attachment of a paramagnetic spin probe to a desired site in a biomolecule. Until a few years ago, the only available choice for protein samples was a nitroxide-based spin label targeting cysteines via functional groups such as methanethiosulfonate, maleimide and iodoacetamide.[1] Nowadays, the expansion of the sensitivity and versatility of pulsed EPR dipolar spectroscopy allows using metal-based labels and carbon-center radicals, which are spectroscopically orthogonal to nitroxide probes to extract interspin distances (a few examples can be found in Ref. [2]).

The biocompatible gadolinium-based labels in particular, are promising to study spin-labeled proteins in mammalian cells (for example see Ref. [3]). Trityl labels are also shown to be resistant in oocytes.[4] However, with respect to gadolinium or trityl labels, nitroxide labels for protein studies in a cellular context could provide several advantages: i) side chain dynamics can be detected and compared with a large literature dataset;[1] ii) interspin distance determination is facilitated by a large modulation depth in double electron-electron resonance (DEER,[5] also known as PELDOR[6]); iii) commercial Q-band spectrometers are optimal for achieving high sensitivity in nitroxide-nitroxide DEER;[7] iv) the small molecular size of nitroxides produces smaller interference with the proteins' structure and function at most sites; v) the water accessibility of the spin-labeled side chain can be measured with X-band continuous wave (cw) EPR and in particular with the newly developed Overhauser dynamic nuclear polarization techniques (ODNP);[8] vi) finally, nitroxide labels can be used orthogonally to other spin probes.

For *in-cell* EPR-experiments on spin-labeled proteins, two methods have been explored: i) The expression of proteins with unnatural amino acids either containing an intrinsic stable paramagnetic center[9] or enabling specific reactions with spin labels in living cells;[10] ii) The insertion of a spin-labeled recombinantly-produced protein into cells via hypotonic swelling, electroporation,[3,11] or micro-injection into oocytes.[12]

For both cases it is mandatory that the spin probes survive the reducing conditions of the cytosol and that labeling does not interfere with proteins' fold, activity or interactions. It is well established that common nitroxides are reduced rapidly in the presence of reducing agents, with a five-membered (pyrrolidine or pyrroline) ring structure being more stable than a six-membered one (piperidine).[13] Therefore, they are not suitable for *in-cell* EPR measurements, unless strategical "tricks" are used, such as working with cell strains with less reducing agents, spin labeling outer membrane proteins, incubating

[a] Dr. S. Bleicken, T. E. Assafa,+ C. Elsner, Prof. Dr. E. Bordignon
Faculty of Chemistry and Biochemistry, Ruhr University Bochum, Universitaetsstrasse 150, 44801 Bochum, Germany
E-mail: enrica.bordignon@rub.de
[b] Dr. H. Zhang,+ Dr. S. Rajca, Prof. Dr. A. Rajca
Department of Chemistry, University of Nebraska, Lincoln, Nebraska 68588-0304, USA
E-mail: arajca1@unl.edu
[c] Dr. S. Bleicken
ZEMOS, Ruhr University Bochum, Universitaetsstrasse 150, 44801 Bochum, Germany
[d] I. Ritsch, Prof. Dr. G. Jeschke
ETH Zurich, Laboratory of Physical Chemistry, Vladimir-Prelog-Weg 2, CH-8093 Zurich, Switzerland.
[e] Dr. M. Pink
IUMSC, Department of Chemistry, Indiana University, Bloomington, Indiana 47405-7102, USA
[+] These authors contributed equally to this work.

Supporting information for this article is available on the WWW under https://doi.org/10.1002/open.201900119

spin-labeled proteins with isolated organelles, etc..[9,14] Surprisingly, it was reported that an unnatural amino acid carrying a five-membered nitroxide can partially survive *E. coli* cell conditions[9]. Wee will address later under which experimental conditions the latter conclusion was reached.

However, as the conventional nitroxide labels mainly performed poorly in living cells, a new generation of sterically shielded nitroxide radicals was developed, which showed an improved resistance against reducing agents such as ascorbic acid and chemicals contained in cellular extracts or oocytes.[15] Confirming these first promising results, recently, the first protein spin labeled with a maleimide functionalized *gem*-diethyl nitroxide was shown to retain its signal after injection into oocytes.[16]

We ask here if, despite being promising, the available data may not be sufficient to declare the *gem*-diethyl nitroxides biocompatible. Ideally, spin-labeled proteins should be studied in their native environment, namely, in the cells they originated from. Xenopus oocytes, which were mostly used to test *gem*-diethyl nitroxides, are large, highly specialized cells full of yolk and very different from all somatic cells. For most proteins, Xenopus oocytes can be useful models to study crowding effects, but to address labels' biocompatibility, different cells should be tested. The majority of available PDB structures of proteins are from humans or other mammals, followed by *E. coli* or *S. cerevisiae* (based on www.rcsb.org). Those are the species to be tested to address biocompatibility of the new labels. Here we will test *E. coli* cell cytosols and highlight their different properties with respect to solutions of ascorbic acids or oocytes in terms of reducing agents. Additional data obtained on human cells are presented elsewhere.[17]

From the spin labeling point of view, we decided to study here a iodoacetamide-functionalized *gem*-diethyl nitroxide (called IAG) and compare it with a maleimide-functionalized *gem*-diethyl nitroxide (called here MAG), which was previously synthesized and characterized in oocytes (and called M-TETPO).[16] The advantages of having two distinct functional groups specific for cysteines at pH close to 7.5 (at different pH values other amino acids could be labeled) and bound to the proteins via an uncleavable S–C bond are explained as follows. First, each protein site has its distinct properties in terms of label accessibility, sensitivity to point mutation, steric constraints, electrostatic properties, water-membrane exposure, etc. Therefore, to maximize the success of the labeling strategies, it is advantageous to have chemically diverse functional groups, and spin labels of different size and flexibility. Second, maleimide groups have some drawbacks, which could be detrimental in the cellular context: i) the thiol adducts to maleimide, i.e., succinimidyl thioethers, can undergo a slow reverse Michael addition, favored by the reducing environment, and thus releasing the spin label;[18] ii) the succinimidyl thioethers can undergo an irreversible pH-dependent hydrolysis to the corresponding succinamic acid thioethers, thus leading to multiple thiol adducts;[19] iii) the addition of the SH group (from the cysteine) to the maleimide ring forms a chiral center (Table 1), so that the resulting spin-labeled amino acid will be present as two diastereomers (or epimers), which makes the interpretation of distances based on rotamer libraries more cumbersome.

Table 1. Calculated partition coefficients (cLogP) and the Connolly solvent excluded volumes (Vol) for MTSL and its *gem*-diethyl analogous with three distinct linkers to Cys).[a]

	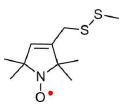 MTSL	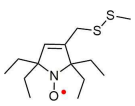	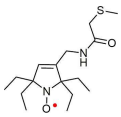	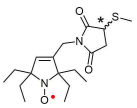
cLogP	2.20	4.31	2.23	3.29
Vol [Å^3]	225	297	319	351

[a] Geometries are optimized using MM2. The star denotes the chiral center created by binding of the cysteine SH group to the maleimide ring. The maleimide functionalized label has been previously synthesized and called M-TETPO.[16]

Here, we used MAG and IAG to label two water soluble proteins (T4 lysozyme and Bid) and compared their properties to the conventional methanethiosulfonate nitroxide label (MTSL, also called R1 once bound to a protein). Two double-cysteine proteins were studied with three different labels and evaluated determining labeling efficiency, site chain mobility and inter-spin distances. Additionally, to appraise the potential use of IAG and MAG in structural studies, rotamer libraries compatible with the MMM software[20] were created and tested on the available data. Finally, the resistance against the reducing agents present in *E. coli* cytosol was probed and compared to ascorbate treatment. Surprisingly, despite being chemically resistant to ascorbic acid, none of the tested *gem*-diethyl labels is compatible with *E. coli* cells at micromolar concentrations.

Results and Discussion

Synthesis of the Spin Labels and Characterization

Here, we report the synthesis of the iodoacetamide *gem*-diethyl spin label **1** (called IAG) and the maleimide *gem*-diethyl spin label **2** (called MAG) (Figure 1).

Properties of *gem*-diethyl nitroxide spin labels, with different linkers targeting cysteines (methanethiosulfonate, maleimide

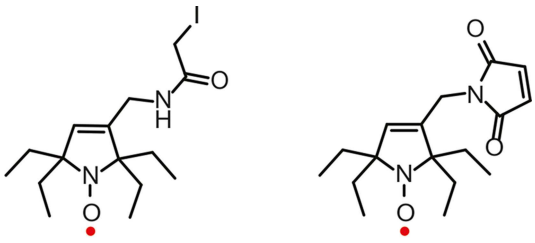

Figure 1. Spin labels **1** (called IAG in the following) and **2** (MAG).

and iodacetamide) are compared in Table 1. We calculated the partition coefficients (cLogP, predicting the hydrophobicity) and the Connolly solvent excluded volumes (Vol, related to the molecular volume), of the MM2-optimized sub-structures of the Cys-bound MTSL and three *gem*-diethyl analogues, with distinct side chain linkers. Both hydrophobicity and molecular volume are significantly increased by the *gem*-diethyl groups.

Our synthesis of spin labels **1** (IAG) and **2** (MAG) (Figure 1) starts from the previously reported mesylate nitroxide **3**,[15b] which was converted to amino nitroxide **5** in 2 steps according to the procedure for the analogous *gem*-dimethyl nitroxides (Scheme 1, SI).[21]

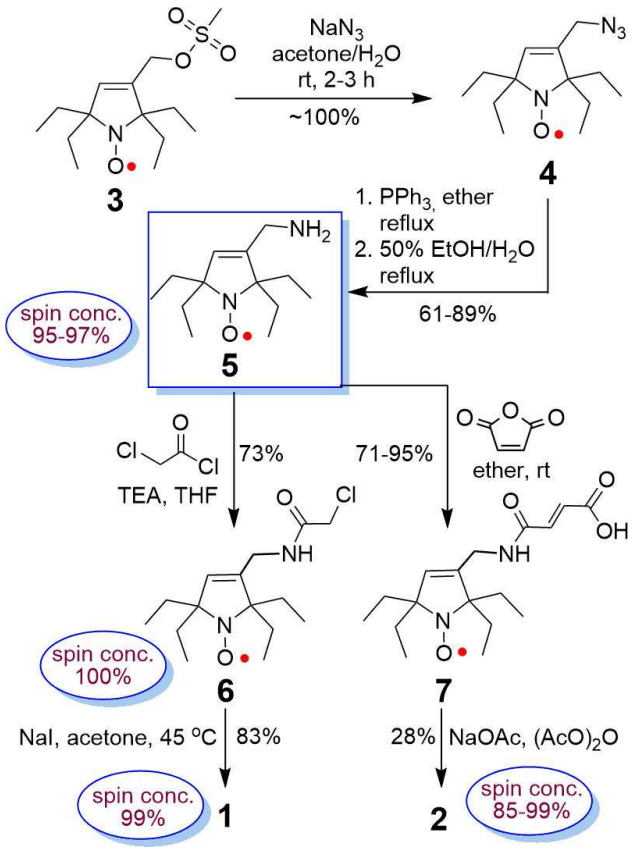

Scheme 1. Synthesis of spin labels 1 and 2. Isolated yields are reported.

Subsequently, **5** was reacted with chloroacetyl chloride, to give nitroxide **6**, which was then converted to spin label **1** via S_N2 reaction with iodide.[22] To prepare spin label **2**, amino nitroxide **5** was reacted with maleic anhydride, and then, the resultant crude mixture of maleamide nitroxide **7** was condensed to maleimide nitroxide **2**, following the procedure for the analogous *gem*-dimethyl spin label[16,23] (Scheme 1). Purity of nitroxides **1**, **2**, **5**, and **6** was confirmed by paramagnetic ^{1}H NMR spectra and EPR-derived spin concentrations.[15d] The identity of the two spin labels was also confirmed by IR and HRMS (see SI). Detailed experimental procedures for the synthesis can be found in the SI.

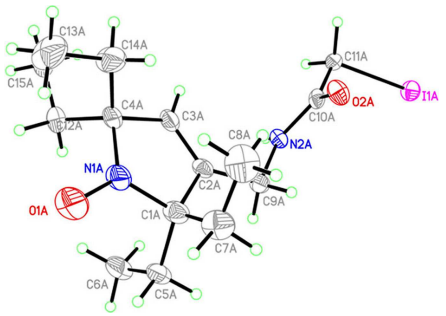

Figure 2. X-ray structures of spin label IAG with molecule A shown only. Carbon, nitrogen, oxygen, and iodine atoms are depicted with thermal ellipsoids set at the 50% probability level. More details may be found in Tables S1/S2 and Figures S5/S6 in the SI.

EPR spectra of IAG (**1**) and MAG (**2**) in chloroform at room temperature showed typical nitroxide spectral parameters, e.g., $g_{iso} = 2.0057$ and $A_{iso}(^{14}N) = 40.5$ MHz.[15d] The radical content was found to be 99% and 85–99% for nitroxides IAG (**1**) and MAG (**2**), respectively, based on spectral double integration (SI).

The structure of spin label **1** (IAG) was confirmed by single-crystal X-ray analysis (Figure 2). In the crystal, two crystallographically distinct but chemically equivalent molecules of **1**, A and B, are found; in molecule B, iodine is disordered over two sites (96/4).

Spin Labeling Tests on Two Water Soluble Proteins: Labeling Efficiency, Side Chain Dynamics and Interspin Distances

We tested the labeling capabilities of IAG and MAG on two water soluble proteins in aqueous buffer at pH 7.5 and compared the results with the commonly available methanethiosulfonate spin label (MTSL or R1 when bound to a protein). Our first test probe was T4 lysozyme carrying two cysteines at positions 131 and 72, which were already extensively studied.[24] The protein was labeled with the three nitroxide spin labels with labeling efficiency of 90–100% (estimated error ±10%). Our second test probe was the proapoptotic protein Bid, which is also structurally well described[25] and contains two native cysteines (positions 30 and 126) which were previously labeled with MTSL.[7,26] Bid was labeled with MTSL, IAG and MAG, with labelling efficiencies of 80, 20 and 80% (±10%), respectively.

The labeling efficiency depends on the labeled sites and the type of label, as illustrated by the differences obtained between T4 lysozyme and Bid. Therefore, the availability of two differently functionalized labels will be advantageous in the optimization of labeling strategies of new proteins. For example, MAG is shown here to label Bid better than IAG, but IAG was found to be optimal for a different apoptotic protein, Bax, in another study.[17]

Figure 3A shows the cw EPR spectra of spin-labeled T4 lysozyme. Each spectrum encodes the characteristic dynamics of the spin-labeled side chain, which are found to be similar for all three labels. The cw spectra of Bid_{R1}, Bid_{MAG} and Bid_{IAG} show two components, with ratios depending on the chosen label

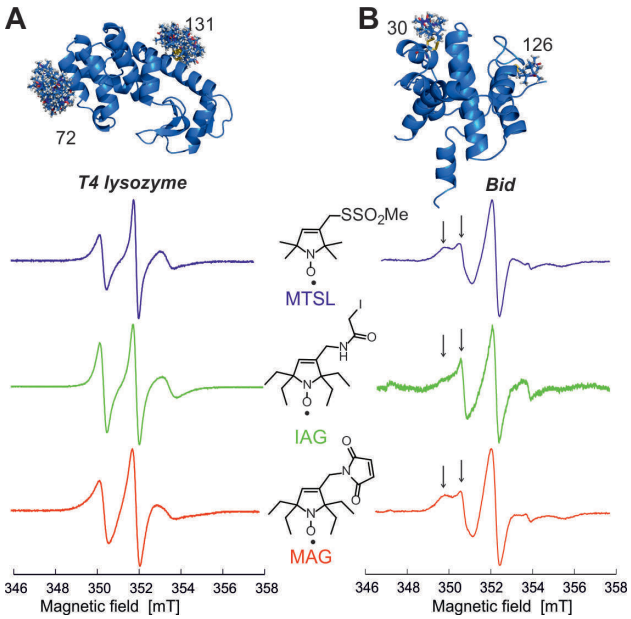

Figure 3. cw EPR spectra of T4-lysozyme and Bid. A. Room temperature X-band cw EPR spectra of T4 lysozyme spin labeled with three different nitroxide labels. The X-ray structure of T4 lysozyme (PDB:1 L63) labeled at position 72 and 131 with MTSL is shown. The room temperature rotamer library of MMM2018.2 was used. B) Room temperature X-band cw EPR spectra of Bid spin labeled with three different nitroxide labels. Arrows highlight the two spectral components. One NMR model of mouse Bid (PDB: 1DDB) labeled at position 30 and 126 with MTSL is shown. (Bid reproducibility data in Supp. Figure 21).

(Figure 3B). For both investigated proteins, we can conclude that IAG and MAG retain the ability to describe site-specific motion of the spin-labeled side chain, and, at least for the sites investigated, their spectral features resemble those obtained with MTSL.

We then addressed how IAG and MAG report on the distances between two sites using Double Electron-Electron Resonance (DEER) spectroscopy. We address if the longer and bulkier linker and the higher steric constraints imposed by the ethyl groups, may affect the distance distributions compared to MTSL. The three nitroxide-labeled T4 lysozyme samples show a distinct distance peak, centered at 3–4 nm (Figure 4A). The modulation depth is around 0.4, as expected from the high labelling efficiency. Intriguingly, the IAG label shows the narrowest distance distribution.

Next, DEER measurements were carried out on the three spin-labeled Bid variants. Bid_{R1} is characterized by a bimodal distance distribution peaking at 2.1 and 2.7 nm, in agreement with previous data.[7,26] Bid_{MAG} and Bid_{IAG} have a monomodal distance distribution centered at around 3 nm.

New Rotamer Libraries and Interspin Distance Simulations

In order to compare the experimental distances with the proteins' structures, softwares are available to attach *in silico* a spin label to an existing PDB structure and simulate the most probable inter-spin distances using rotamer libraries. Here we provide new rotamer libraries for *gem*-diethyl labels compatible with the MMM[20a] software, generated by an extended version of the approach previously used for other nitroxide and for Gd (III) labels.[14c,20a,27]

Briefly, initial structures of the labels were obtained by unrestricted Kohn-Sham DFT using the B3LYP functional and

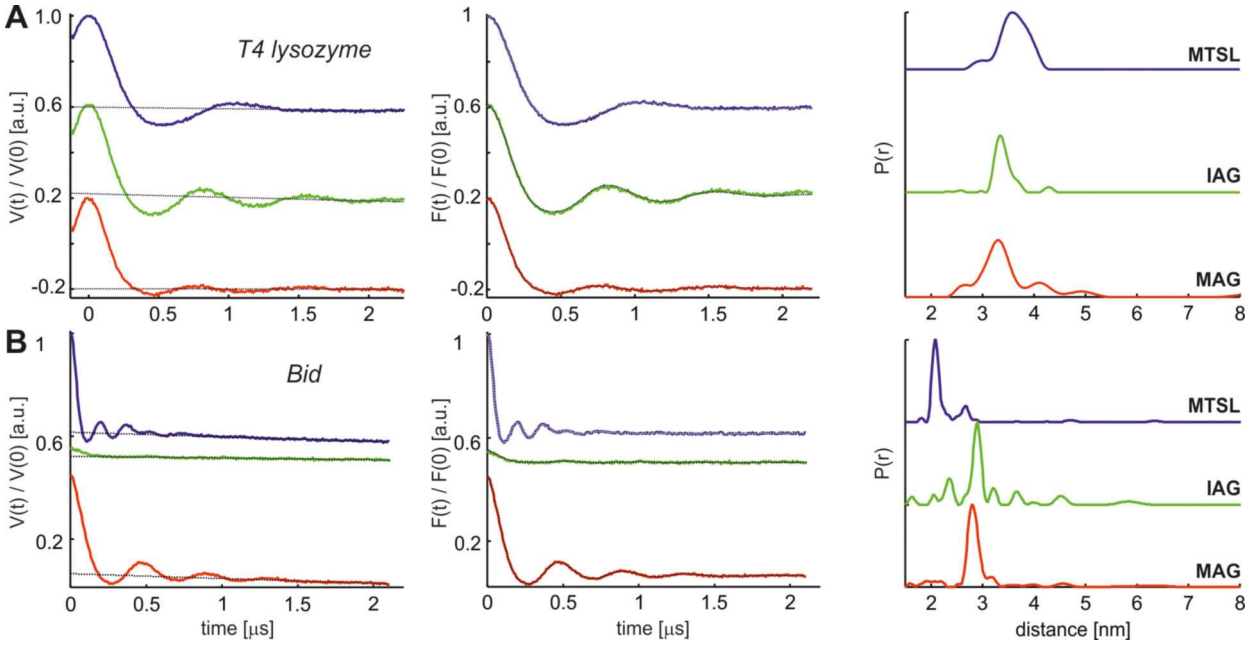

Figure 4. DEER analysis of T4 lysozyme (A) and Bid (B). Left: primary Q-band DEER data and background function; center: background corrected traces with fit via Tikhonov regularization; right: obtained distance distributions.

def2-SVP basis set in ORCA.[28] Rotamers of the linker between the protein backbone and the nitroxide heterocycle were found by sampling conformation space at fixed bond lengths and angles using the torsion and non-binding interaction potentials of the UFF force field.[29] The van-der-Waals radii were scaled by a forgive factor of 0.9. In this step, ensembles of 2×10^4 conformations were generated, which were then hierarchically clustered to 72 rotamers for MAG and 243 rotamers for IAG (level 1 library). For each of these labels, generation of level 1 libraries was attempted for all 81 possible combinations of ethyl side group rotamers (3 rotamers per ethyl group). Combinations, where the ethyl groups clash among themselves were skipped. For MAG, which has a chiral linker in addition to the chiral Cα atom, this procedure was repeated for the other diastereomer. All level 1 libraries for a label were then combined into a single library (level 2 library). Level 2 libraries are very large: 4176 rotamers for MAG and 6561 rotamers for IAG. We found that the number of rotamers can be reduced without significantly affecting predicted distance distributions. For this, we culled level 2 libraries by removing all rotamers that had populations smaller than 0.1% or 0.2% of the maximally populated rotamer for MAG and IAG, respectively. The resulting level 3 libraries include 1367 and 2461 rotamers for MAG and IAG, respectively.

Initially, we computed the interaction of the rotamers with the protein as described previously.[20a] However, we found that predictions for MAG and IAG were significantly off with respect to the available experimental distances. We hypothesized that a forgive factor of 0.5 for both the attractive and repulsive part of the Lennard-Jones non-bonding interaction potential is not a good approximation for labels that feature four hydrophobic ethyl groups. In order to test this hypothesis, we multiplied the attractive component of the Lennard-Jones potential by a variable factor.

For both labels and both proteins, we found the best agreement of predicted and experimental distance distributions when enhancing attraction energy by a factor of 2. Rotamer libraries for MAG and IAG are implemented in MMM2018.2 with this enhancement of the attraction potential.

The results of the simulations with the new libraries are shown in Figure 5. We observed a good agreement between simulated and experimental mean distances (Figure 5A) in T4 lysozyme when using MTSL on four PDB structures (the rmsd between simulated and experimental mean distances lies in the expected 0.3–0.4 nm range[30]). Notably, MAG libraries had a similar performance as MTSL, while the distance distributions simulated with IAG deviated more between the four structures, possibly due to its longer linker (Figure 5A–B).

For Bid, we analyzed the 20 available NMR models, and observed that the agreement between experimental and simulated distances depends strongly on the model chosen for all labels (Figure 5C–E). Bid is a protein composed of 8 alpha helices, which are relatively rigid based on the NMR structures. However, the models clearly differ in the orientations of the termini and the loops (Figure 5D). Thereby, cys30 is placed in a loop and cys126 next to a loop (Figure 5D). We observed large differences between the location of the rotamers populated in different models, especially at position 126, for which only few rotamers are populated. The large variation in the rotamers' orientation in model #9 and #15 are presented for IAG at

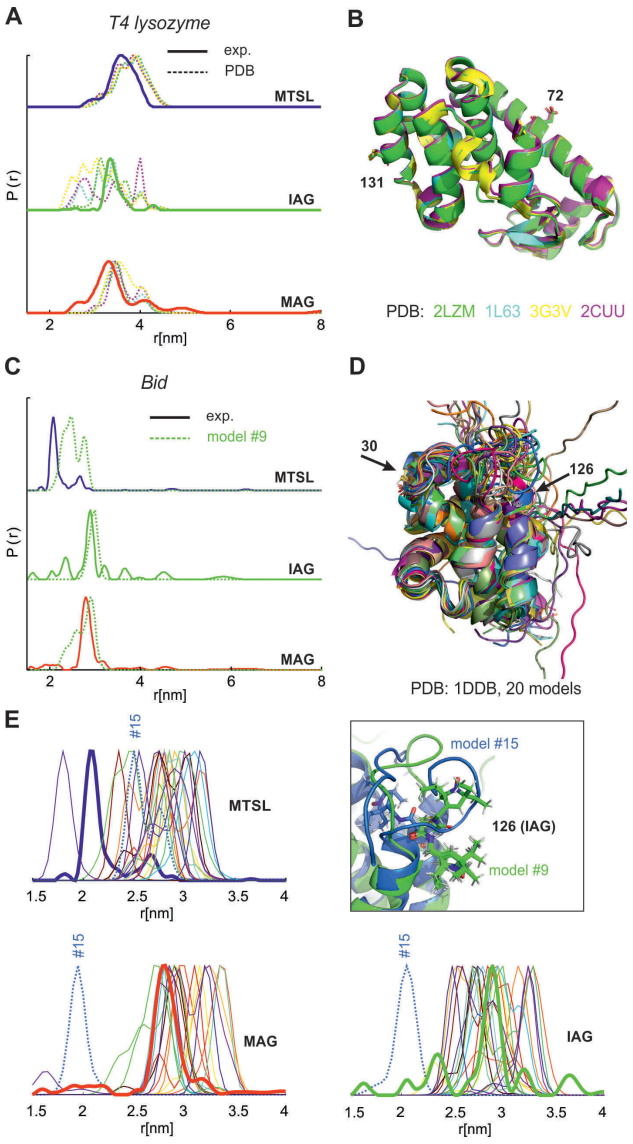

Figure 5. Rotamer library simulations. A) T4 lysozyme interspin distances were calculated using the available room temperature rotamer libraries of MTSL, IAG and MAG in MMM2018.2. Four representative crystal structures were used. PDB: 2LZM is a high-resolution structure of T4 lysozyme wild type; 1 L63 the structure with cysteine amino acids replaced 3G3 V and 2CUU a high and low temperature structure of the protein spin labeled at position 131, without cysteines. B) The four X-ray structures are superimposed and the spin-labeled sites highlighted. C) Simulated distance distributions for Bid. A good agreement between experimental and simulated distances was found to be achieved for the NMR model 9 for all spin labels (green dotted). D) The NMR structure of Bid (PDB:1DDB) consists of 20 models, which were used for the calculation. The two natural cysteines used for labeling are highlighted. E) The distribution of distances simulated on the 20 models (dotted) highlight model-based differences. The experimental data are shown as thick colored lines. The few populated rotamers at position 126 are affected by different modeling of the neighbouring loop. The NMR model#15 is an outlier for MAG and IAG, and the inset shows how the different location of the loop close to position 126 is the reason for a completely different localization of the IAG rotamers with respect to the other models (model #9 is shown as reference).

position 126 (inset in Figure 5E). Considering all 3 spin labels, model #9 of Bid showed the best agreement with the experimental data, while model #15 the worst (Figure 5E). We can therefore conclude that the first tests using the new IAG and MAG libraries were successful.

Resistance to Reducing Agents in *E. coli* Cells

As mentioned before, *gem*-diethyl substituted nitroxides as well as a MAG-labeled protein were reported to be more stable based on experiments using ascorbate or Xenopus oocyte extracts.[15b–d,16] Based on this, MAG was assumed to be biocompatible. However, ascorbate is not the main reducing chemical in cells and Xenopus oocytes are highly specialized cells not comparable to somatic cells of any species. Therefore, to investigate if IAG and MAG are truly compatible with prokaryotic cells, we cultivated *E. coli* cells and isolated their cytosol (Figure 6A and SI). This cytosol as well as an ascorbate solution were used to test the stability of different nitroxide probes: TEMPOL, 3-carboxy PROXYL, *gem*-diethyl pyrroline, Bid_{R1}, Bid_{MAG} and Bid_{IAG}. In our experiments, *gem*-diethyl pyrroline at 50 μM spin concentrations proved to be more stable against ascorbate (50 mM) than TEMPOL or 3-carboxy proxyl (Supp. Figure 22A) in agreement with previous findings.[15c,d] Additionally, at similar spin concentrations, Bid_{MAG} and Bid_{IAG} proved to be more stable against ascorbate than Bid_{R1} (Supp. Figure 22B). Thereby, the labels attached to the proteins were slightly more stable as the free labels, possibly due to steric constraints imposed by the neighboring side chains.

Surprisingly, in presence of *E. coli* cytosol all six probes/proteins decayed rather fast, as can be clearly seen by comparison of the cw spectra at different incubation times (Figure 6B, 7A). The *gem*-diethyl groups provided only a very slight advantage over the *gem*-dimethyl groups (Figure 6B, 7A, and Supp. Figure 23). To qualitatively follow the signal decay, we plotted the intensity of the central line versus time (Figure 6B, 7A). At comparable spin concentrations, the labels attached to Bid (Figure 7A) decayed a bit slower than the free labels (Figure 6B).

Notably, for the Bid_{IAG} sample that contains residual free label, we detected a faster reduction of the free versus the bound labels (see fast decay in the first minutes in the plot of Figure 7A and Supp. Figure 24). We found that the signal decay of Bid_{IAG} was reproducibly slower than Bid_{MAG} (Table S3), probably due to a better shielding induced by the neighboring sidechains (correlated with the overall lower labeling efficiency of IAG with respect to MAG).

Based on our kinetics, the *gem*-dimethyl nitroxide probes are not stable in *E. coli* cells. However, Schmidt *et al.* described the use of unnatural amino acids carrying a *gem*-dimethyl nitroxide incorporated into proteins in *E. coli* cells, on which *in vitro* and *in-situ* EPR measurements were performed.[14f] There, millimolar spin concentrations were added to the *E. coli* cells. We addressed the effects of increasing the spin concentration in cells by varying the ratio of spin-labeled Bid to the *E. coli* cytosol (Figure 7B). We cannot concentrate Bid at high millimolar concentration due to aggregation problems. However, by further diluting the cytosol we achieved a similar spin-to-reducing agent ratio as in millimolar protein concentrations in the *in-cell* experiment mentioned above. To estimate the

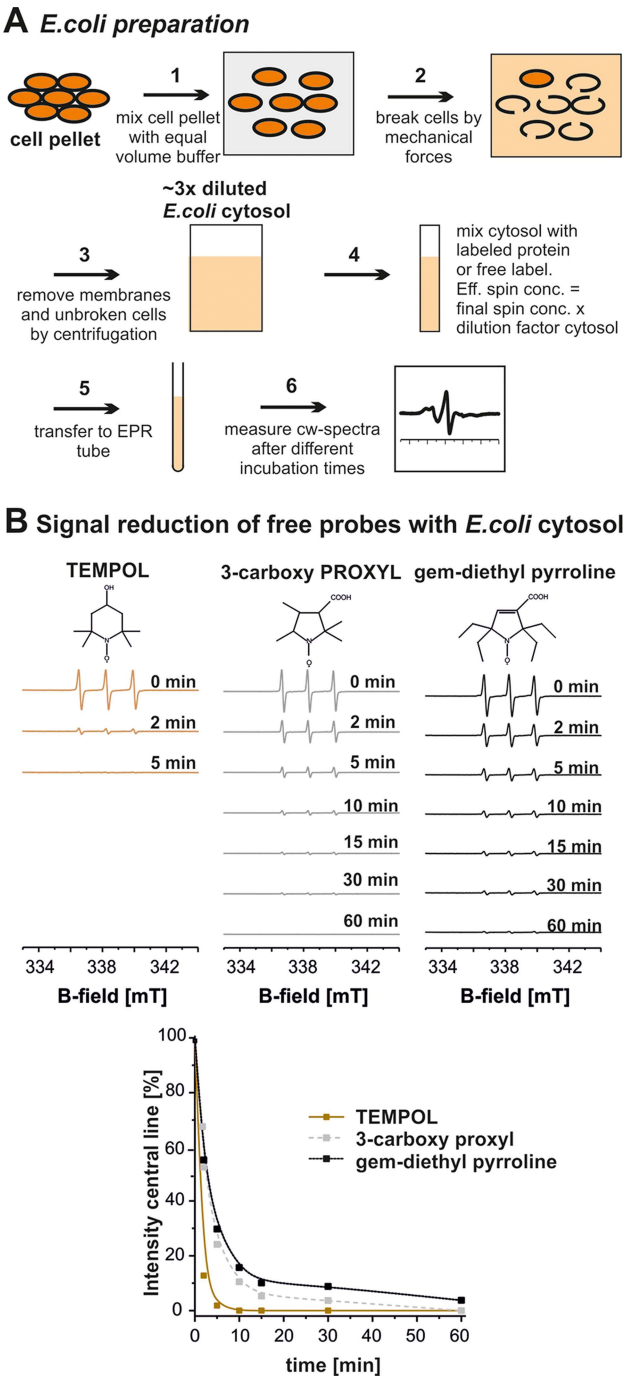

Figure 6. Radical stability in *E. coli* cells. A) Scheme of the preparation of *E. coli* cytosol and its dilution. The 3x dilution factor is an approximated value taking into account the membrane volume, and possible losses during centrifugation. B) cw EPR room temperature spectra detected at different incubation times indicated in the figure. Final spin concentration: 50 μM, dilution factor 6x for the cytosol. Right: qualitative decay curve obtained by plotting the intensity of the central line versus time. The 100% reference is the intensity of the signal obtained on the same sample diluted with pure buffer (see SI).

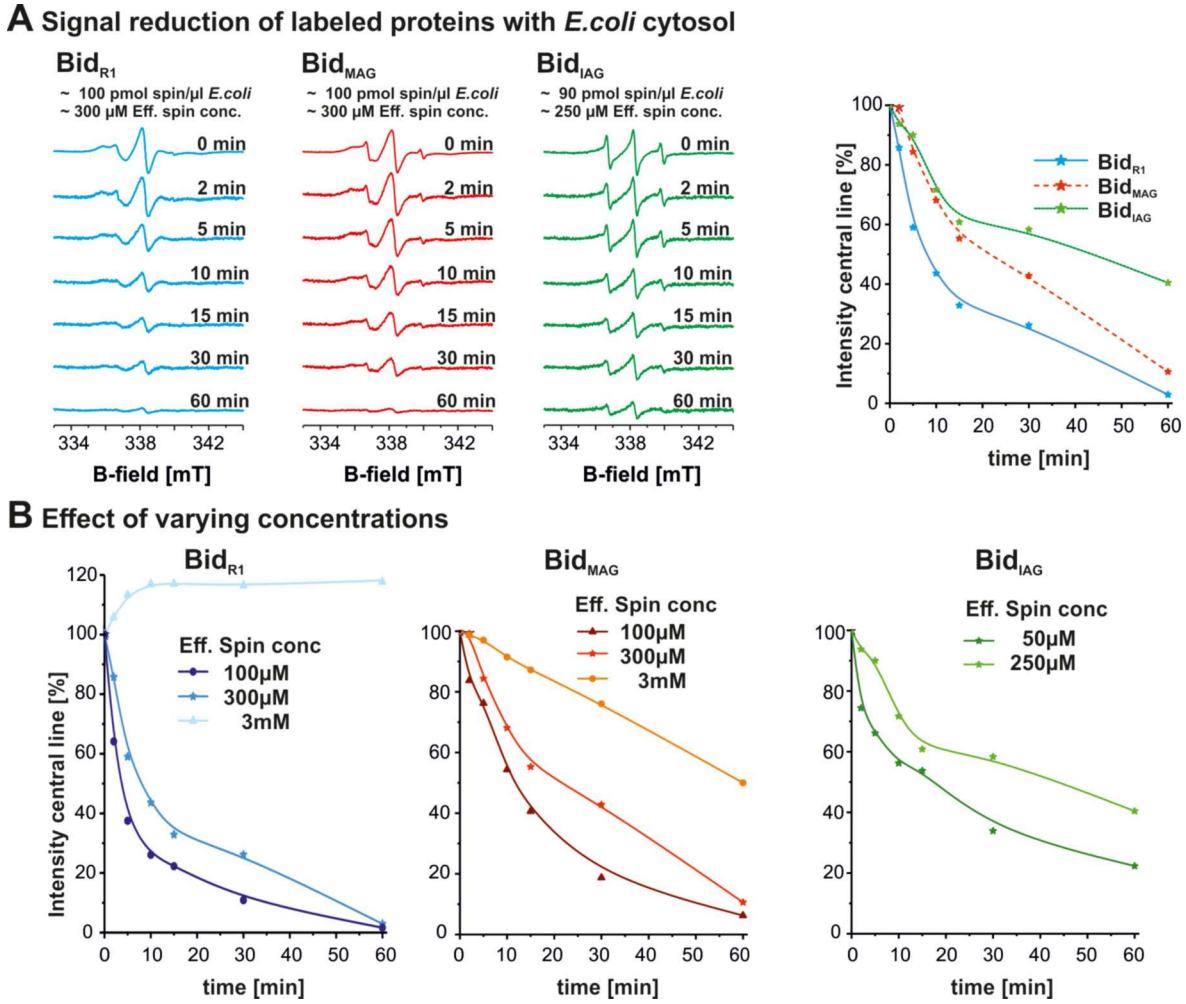

Figure 7. Stability of the spin-labeled side chain in *E. coli* at different concentrations. A) Signal reduction of 20 µL sample containing: Bid_{R1} (10 µL of 100 µM spin plus 10 µL cytosol 3x diluted), Bid_{MAG} (10 µL of 100 µM spin plus 10 µL cytosol 3x diluted) and Bid_{IAG} (17.5 µL of 12.5 µM spin plus 2.5 µL cytosol 3x diluted). The moles of spins per microliter of added cytosol (E. c.) and the effective spin concentrations are indicated (see SI and Supp. Figure 23). The fast decay in Bid_{IAG} within the first 20 minutes is attributed to the faster reduction of the free label in the solution with respect to the bound one (Supp. Figure 24). B) Effects induced by increasing the "effective" spin concentration on the signal reduction curves. The increase in signal intensity observed for MTSL is due to the release of the label from the protein at high spin concentration, which created the characteristic three narrow lines in the spectrum (see Supp. Figure 23).

putative intracellular spin concentration, we calculated an "effective" spin concentration, which is the actual final spin concentration (c_{spin}) multiplied by the dilution factor of the *E. coli* cytosol (3 $V_{tot}/V_{cytosol}$) (see SI).

At the lowest effective spin concentration used (50–100 µM) all three nitroxide labels are reduced by more than 80% within one hour (Figure 7B). At 250–300 µM (Figure 7B, also shown in Figure 7A) the reduction curve is already slower. At an effective spin concentration of ~3 mM the spin reduction is further slowed down and in case of MTSL, label release is visible (Figure 7B and Supp. Figure 23). Notably, the MAG or IAG labels offer only one target for chemical reduction, namely the NO radical, while MTSL can have also the S–S bond reduced, so potentially, MTSL uses more reducing agents than the other two labels. At millimolar spin concentration the reducing agents of the *E. coli* cells cannot completely reduce all spin labels, which explains previously published results obtained with millimolar nitroxide concentrations in cells.[14f] Of note, millimolar protein concentrations largely exceed physiological conditions. Therefore *in-cell* experiments targeting physiologically-relevant concentrations of spin-labeled recombinant proteins must rely on micro- to sub-micro-molar protein concentrations.

Based on the data available, we surmise that *E. coli* cells have enough reducing agents to silence micro- but not millimolar spin label concentrations. In summary, none of the tested spin labels is compatible with *E. coli* cells at physiological protein concentrations and these results are confirmed also using a different spin-labeled protein.[17]

Conclusions

The *gem*-diethyl nitroxide spin labels IAG and MAG are suitable for labeling accessible cysteines in proteins and provide valuable mobility information by cw EPR spectroscopy at

physiological temperatures and interspin distances by DEER spectroscopy. For the two cases studied here, IAG and MAG were characterized by interspin distances with monomodal distributions and narrow width. Both properties are favourable for protein studies in cellular context and could be satisfactorily simulated with the new rotamer libraries. Additional studies will be needed to verify if the steric constraints imposed by the ethyl groups generally favour a more homogenous localization of the nitroxide group with respect to the protein backbone. The labeling efficiency of IAG and MAG is shown to be protein- and site-specific, however we think that at similar labeling efficiencies, IAG is in principle superior as it does not suffer from the creation of uncontrolled mixtures of diastereomers. The availability of two *gem*-diethyl spin labels targeting cysteines with different functional groups and their rotamer libraries will aid finding the optimal strategies for protein studies. Both labels are shown to be very resistant to reducing agents such as 50 mM ascorbate, but cannot sustain incubation with *E. coli* cell extracts, unless used at millimolar concentration. Therefore, their use for *in-cell* EPR is still challenging, and optimal cell lines and strains, spin concentrations and incubation times should be optimized for each foreseen project. The next target for these new labels is mammalian cells, which may have different types and concentrations of reducing agents, which need to be thoroughly investigated. Work is in progress to study the response of *gem*-diethyl nitroxide labels in those cells.[17]

Experimental Section

X-Ray Crystallography of Spin Label 1

A small, colorless crystal was measured with synchrotron radiation ($\lambda = 0.41328$ (30 keV), at 100(2) K with a frame time of 0.3 seconds. Two sets of frames were collected and integrated (SAINT, Bruker Analytical X-Ray Systems, Madison, WI, 2016) yielding a total of 37690 reflections to a maximum θ angle of 16.02°, with 8110 independent and 5848 observed [$2\sigma(F^2)$] reflection. The final cell constants of $\underline{a} = 9.1567(6)$ Å, $\underline{b} = 23.5606(16)$ Å, $\underline{c} = 16.8041(12)$ Å, $\beta = 100.1048(19)°$, volume = 3569.0(4) Å^3, are based upon the refinement of the XYZ-centroids of 7329 reflections above 20 σ(I) with $4.879° < 2\theta < 31.83°$. Data were corrected for absorption effects using the multi-scan method (SADABS, Bruker Analytical X-Ray Systems, Madison, WI, 2016). The material crystallizes in the monoclinic space group $P2_1/c$. The structure was solved with intrinsic methods and refined using the SHELX suite of programs.[31] All non-hydrogen atoms were refined with anisotropic displacement parameters. The hydrogen atoms were placed in ideal positions and refined as riding atoms with relative isotropic displacement parameters. Hydrogen atoms involved in NH…O hydrogen bonds were refined for all parameters. Larger than average displacement indicated for I1B positional disorder for the atom, which refined to a 96:4 site occupancy ratio. The final anisotropic full-matrix least-squares refinement on F^2 with 381 variables converged at R1 = 4.75 %, for the observed data and wR2 = 14.93 % for all data. The goodness-of-fit was 1.050. The largest peak in the final difference electron density synthesis was 1.269 e$^-$/Å^3 and the largest hole was −2.014 e$^-$/Å^3 with an RMS deviation of 0.238 e$^-$/Å^3. The structure was deposited at the Cambridge Crystallographic Data Centre: CCDC 1851693.

Proteins and *E. coli* Cytosol Preparation

T4 lysozyme and Bid purification methods are described in the SI. Spin labelling was performed in aqueous buffers at pH 7.5 and 7.6. Further details about the cytosol preparation from *E. coli* cell cultures are given in the SI.

Labeling Efficiency and EPR Measurements

The cw EPR spectra were obtained using a Miniscope 5000 X-band spectrometer (Magnettech by Freiberg Instruments). The sample (20 µl) was inserted into glass capillaries (0.9 mm I.D. inner diameter). The spectra shown in Figure 3 were detected with 15 mT field sweep, 0.15 mT modulation amplitude and 10 mW microwave power, while the spectra in Figure 6 and 7 and Supp. Figure 21–24 used a 12 mT field sweep. The spin concentration was calculated by comparison of the double integral of the protein spectrum with that of a reference sample (100 µM TEMPOL in water) and the labeling efficiency was determined as a percentage ratio between spin and protein concentration.

For DEER experiments, 33 % or 50 % (v/v) of deuterated glycerol was added as cryoprotectant to the samples yielding a final protein concentration of 15–20 µM for Bid and 20 µM for T4 lysozyme, respectively. 50 µl aliquots were transferred into 3 mm outer diameter quartz tubes and flash-frozen in liquid nitrogen. Q-band DEER measurements were performed at 50 K on a Bruker ELEXSYS E580 with a separate electron–electron double resonance (ELDOR) source or an arbitrary waveform generator (AWG) with a 150 W traveling wave tube (TWT) amplifier and a homemade resonator. A 4-pulse DEER sequence with 100 MHz separation between the pulses was applied with 12 ns rectangular pulses (for T4 lysozyme) or 14 ns full width at half maximum Gaussian pulses (for Bid) for both observer and pump frequencies.[7,32] Additional artefacts in the DEER trace from the coherent AWG generated pulses were removed by 16-step phase cycling. To extract the interspin distance distributions, DEER traces were processed using the DeerAnalysis2016 software, employing mono-exponential background fitting functions and a model-free Tikhonov regularization of the background corrected traces.[33]

Acknowledgements

We thank the National Institutes of Health for support of this work through grant NIGMS R01 GM124310-01 (to AR and SR). NSF's ChemMatCARS Sector 15 is principally supported by the Divisions of Chemistry (CHE) and Materials Research (DMR), National Science Foundation, under grant number NSF/CHE-1346572. Use of the Advanced Photon Source, an Office of Science User Facility operated for the U.S. Department of Energy (DOE) Office of Science by Argonne National Laboratory, was supported by the U.S. DOE under Contract No. DE-AC02-06CH11357. This work was funded by Deutsche Forschungsgemeinschaft (DFG, German Research Foundation) under Germany's Excellence Strategy-EXC-2033-Projektnummer 390677874 (EB), and by the DFG Priority Program SPP1601 "New Frontiers in Sensitivity in EPR Spectroscopy" (EB). EB thanks Remmia Matthews and Benesh Joseph for the expression and purification of T4 lysozyme in ETH Zurich, Laura Galazzo for the reproducibility measurements of Bid and Oliver Oberhänsli from ETH Zurich for the homemade Q-band resonator. SB and CE thank Janine Beermann and Katerina Koutsantas for excellent technical assistance.

Conflict of interest

The authors declare no conflict of interest.

Keywords: biocompatibility · nitroxide · EPR · pyrrolines · spin labeling

[1] E. Bordignon in EPR Spectroscopy of Nitroxide Spin Probes, *eMagRes*, **2017**.
[2] a) M. Yulikov in Chapter 1 Spectroscopically orthogonal spin labels and distance measurements in biomolecules, Vol. 24 The Royal Society of Chemistry, **2015**, pp. 1–31; b) J. J. Jassoy, A. Meyer, S. Spicher, C. Wuebben, O. Schiemann, *Molecules* (Basel, Switzerland) **2018**, *23*, 682; c) B. Joseph, V. M. Tormyshev, O. Y. Rogozhnikova, D. Akhmetzyanov, E. G. Bagryanskaya, T. F. Prisner, *Angew. Chem. Int. Ed. Engl.* **2016**, *55*, 11538–11542; d) Z. Wu, A. Feintuch, A. Collauto, L. A. Adams, L. Aurelio, B. Graham, G. Otting, D. Goldfarb, *J. Phys. Chem. Lett.* **2017**, *8*, 5277–5282; e) T. F. Cunningham, M. R. Putterman, A. Desai, W. S. Horne, S. Saxena, *Angew. Chem. Int. Ed. Engl.* **2015**, *54*, 6330–6334.
[3] F. X. Theillet, A. Binolfi, B. Bekei, A. Martorana, H. M. Rose, M. Stuiver, S. Verzini, D. Lorenz, M. van Rossum, D. Goldfarb, P. Selenko, *Nature* **2016**, *530*, 45–50.
[4] J. J. Jassoy, A. Berndhäuser, F. Duthie, S. P. Kühn, G. Hagelueken, O. Schiemann, *Angew. Chem. Int. Ed. Engl.* **2017**, *56*, 177–181.
[5] G. Jeschke in Dipolar Spectroscopy-Double-Resonance Methods, *eMagRes*, **2016**.
[6] Y. D. Tsvetkov, M. Bowman, Y. Grishin, Pulsed Electron-Electron Double Resonance, *Springer International Publishing* **2019**.
[7] Y. Polyhach, E. Bordignon, R. Tschaggelar, S. Gandra, A. Godt, G. Jeschke, *Phys. Chem. Chem. Phys.* **2012**, *14*, 10762–10773.
[8] I. Kaminker, R. Barnes, S. Han, *Methods Enzymol.* **2015**, *564*, 457–483.
[9] M. J. Schmidt, A. Fedoseev, D. Summerer, M. Drescher, *Methods Enzymol.* **2015**, *563*, 483–502.
[10] S. Kucher, S. Korneev, S. Tyagi, R. Apfelbaum, D. Grohmann, E. A. Lemke, J. P. Klare, H. J. Steinhoff, D. Klose, *J. Magn. Reson.* **2017**, *275*, 38–45.
[11] A. Martorana, G. Bellapadrona, A. Feintuch, E. Di Gregorio, S. Aime, D. Goldfarb, *J. Am. Chem. Soc.* **2014**, *136*, 13458–13465.
[12] I. Krstic, R. Hansel, O. Romainczyk, J. W. Engels, V. Dotsch, T. F. Prisner, *Angew. Chem. Int. Ed. Engl.* **2011**, *50*, 5070–5074.
[13] a) J. F. W. Keana, F. L. Vannice, *Phys Chem Phys Med NMR* **1984**, *16*, 477–480; b) W. R. Couet, R. C. Brasch, G. Sosnovsky, T. N. Tozer, *Magn. Reson. Imaging* **1985**, *3*, 83–88; c) F. Hyodo, K. Matsumoto, A. Matsumoto, J. B. Mitchell, M. C. Krishna, *Cancer Res.* **2006**, *66*, 9921–9928.
[14] a) S. Bleicken, G. Jeschke, C. Stegmueller, R. Salvador-Gallego, A. J. Garcia-Saez, E. Bordignon, *Mol. Cell* **2014**, *56*, 496–505; b) S. Dunkel, L. P. Pulagam, H. J. Steinhoff, J. P. Klare, *Phys. Chem. Chem. Phys.* **2015**, *17*, 4875–4878; c) B. Joseph, A. Sikora, E. Bordignon, G. Jeschke, D. S. Cafiso, T. F. Prisner, *Angew. Chem. Int. Ed. Engl.* **2015**, *54*, 6196–6199; d) R. Igarashi, T. Sakai, H. Hara, T. Tenno, T. Tanaka, H. Tochio, M. Shirakawa, *J. Am. Chem. Soc.* **2010**, *132*, 8228–8229; e) J. Cattani, V. Subramaniam, M. Drescher, *Phys. Chem. Chem. Phys.* **2017**, *19*, 18147–18151; f) M. J. Schmidt, J. Borbas, M. Drescher, D. Summerer, *J. Am. Chem. Soc.* **2014**, *136*, 1238–1241.
[15] a) S. D. Huang, H. Zhang, J. T. Paletta, S. Rajca, A. Rajca, *Free Radical Res.* **2018**, *52*, 327–334; b) Y. Wang, J. T. Paletta, K. Berg, E. Reinhart, S. Rajca, A. Rajca, *Org. Lett.* **2014**, *16*, 5298–5300; c) J. T. Paletta, M. Pink, B. Foley, S. Rajca, A. Rajca, *Org. Lett.* **2012**, *14*, 5322–5325; d) A. P. Jagtap, I. Krstic, N. C. Kunjir, R. Hansel, T. F. Prisner, S. T. Sigurdsson, *Free Radical Res.* **2015**, *49*, 78–85.
[16] G. Karthikeyan, A. Bonucci, G. Casano, G. Gerbaud, S. Abel, V. Thome, L. Kodjabachian, A. Magalon, B. Guigliarelli, V. Belle, O. Ouari, E. Mileo, *Angew. Chem. Int. Ed. Engl.* **2018**, *57*, 1366–1370.
[17] M. Teucher, V. Baader, K. Winklhofer, A. J. Garcia-Saez, H. Zhang, A. Rajca, S. Bleicke, E. Bordignon, submitted **2019**.
[18] a) A. D. Baldwin, K. L. Kiick, *Bioconjugate Chem.* **2011**, *22*, 1946–1953; b) B. Q. Shen, K. Y. Xu, L. N. Liu, H. Raab, S. Bhakta, M. Kenrick, K. L. Parsons-Reponte, J. Tien, S. F. Yu, E. Mai, D. W. Li, J. Tibbitts, J. Baudys, O. M. Saadi, S. J. Scales, P. J. McDonald, P. E. Hass, C. Eigenbrot, T. Nguyen, W. A. Solis, R. N. Fuji, K. M. Flagella, D. Patel, S. D. Spencer, L. A. Khawlil, A. Ebens, W. L. Wong, R. Vandlen, S. Kaur, M. X. Sliwkowski, R. H. Scheller, P. Polakis, J. R. Junutula, *Nature Biotech.* **2012**, *30*, 184–189.
[19] a) S. Suttapitugsakul, H. P. Xiao, J. Smeekens, R. H. Wu, *Mol. Biosystems* **2017**, 13, 2574–2582; b) K. Renault, J. W. Fredy, P.-Y. Renard, C. Sabot, *Bioconjugate Chem.* **2018**, 29, 2497–2513.
[20] a) Y. Polyhach, E. Bordignon, G. Jeschke , *Phys. Chem. Chem. Phys.* **2011**, *13*, 2356–2366; b) G. Jeschke, *Protein Sci.* **2018**, *27*, 76–85.
[21] H. O. Hankovszky, K. Hideg, L. Lex, *Synthesis* **1981**, 147–149.
[22] a) S. Ogawa, H. M. Mcconnell, *Proc. Mont. Acad. Sci.* **1967**, *58*, 19; b) H. M. Mcconnell, W. Dea, R. T. Ogata, *Biochemistry* **1969**, *8*, 2580; c) V. Meyer, M. A. Swanson, L. J. Clouston, P. J. Boratynski, R. A. Stein, H. S. Mchaourab, A. Rajca, S. S. Eaton, G. R. Eaton, *Biophys. J.* **2015**, *108*, 1213–1219.
[23] J. L. Dreyer, H. Beinert, J. F. W. Keana, O. H. Hankovszky, K. Hideg, S. S. Eaton, G. R. Eaton, *Biochim. Biophys. Acta* **1983**, *745*, 229–236.
[24] L. Columbus, T. Kálai, J. Jekö, K. Hideg, W. L. Hubbell, *Biochemistry* **2001**, *40*, 3828–3846.
[25] J. J. Chou, H. Li, G. S. Salvesen, J. Yuan, G. Wagner, *Cell* **1999**, *96*, 615–624.
[26] S. Bleicken, A. J. Garcia-Saez, E. Conte, E. Bordignon, *PLoS One* **2012**, *7*.
[27] E. A. Suturina, D. Häussinger, K. Zimmermann, L. Garbuio, M. Yulikov, G. Jeschke, I. Kuprov, *Chem. Sci.* **2017**, *8*, 2751–2757.
[28] F. Neese, *Wiley Interdis. Rev.: Comput. Mol. Sci.* **2012**, *2*, 73–78.
[29] A. K. Rappe, C. J. Casewit, K. S. Colwell, W. A. Goddard, W. M. Skiff, *J. Am. Chem. Soc.* **1992**, *114*, 10024–10035.
[30] G. Jeschke, *Prog. Nucl. Magn. Reson. Spectrosc.* **2013**, *72*, 42–60.
[31] G. M. Sheldrick, *Acta Crystallogr. Sect. A* **2008**, *64*, 112–122.
[32] M. Teucher, E. Bordignon, *J. Magn. Reson.* **2018**, *296*, 103–111.
[33] G. Jeschke, V. Chechik, P. Ionita, A. Godt, H. Zimmermann, J. Banham, C. R. Timmel, D. Hilger, H. Jung, *Appl. Magn. Reson.* **2006**, *30*, 473–498.

Manuscript received: April 2, 2019